2024 IEEE International Conference on Robotics and Automation (ICRA 2024)
May 13-17, 2024. Yokohama, Japan

Pulsating Fluidic Sensor for Sensing of Location, Pressure and Contact Area

Joanna Jones[1], Marco Pontin[1] and Dana D. Damian[1,2,3]

***Abstract*— Designing information-rich and space-efficient sensors is a key challenge for soft robotics, and crucial for the development of safe soft robots. Sensing and understanding the environmental interactions with a minimal footprint is especially important in the medical context, where portability and unhindered patient/user movement is a priority, to move towards personalized and decentralized healthcare solutions. In this work, a pulsating fluidic soft sensor (PFS) capable of determining location, pressure and contact area of press events is shown. The sensor relies on spatio-temporal resistance changes driven by a pulsating conductive fluid. The sensor demonstrates good repeatability and distinction of single and multiple press events, detecting single indents of sizes greater than 1 cm, forces larger than 2 N, and various locations across the sensor, as well as multiple indents spaced 2 cm apart. Furthermore, the sensor is demonstrated in two applications to detect foot placement and grip location. Overall, the sensor represents an improvement towards minimizing electronic hardware, and cost of the sensing solution, without sacrificing the richness of the sensing information in the field of soft fluidic sensors.**

I. INTRODUCTION

Information-rich and space-efficient sensors are key requirements for many applications, biomedical ones in particular. In the medical context, understanding the environment robots are placed in is essential for safe patient-robot interaction [1]. Receiving information on constraints in the operational space and on how the environment reacts to interactions represents a critical requirement for robots to make informed control decisions. For assistive and rehabilitation devices, improving portability, by minimizing the resources needed for sensing, as well as achieving compact designs, to not hinder the natural movement of the body, are crucial. These have proven to be stringent requirements challenging current sensor technology development [2].

Accurate and precise sensing in soft robotics is commonly accomplished using multiple sensors. However, achieving their seamless integration into robots and wearable devices, without compromising human or robot motion, adding excess weight for users, or being computationally demanding, still requires further exploration. Most common soft sensors have been dedicated to transducing pressure and stretch. This has been achieved using resistive, capacitive, piezoresistive [3], optical [4] and magnetic [5]technologies, mostly embedded in fluidic or conductive stretchable substrates. Distinguishing between stimuli is also a key area of research and, in fluidic sensors, tends to rely on multiple layers of resistive-based conductive liquid layers, with sensitivity to various stimuli derived from the channel shape, capable of differentiating between pressure and strain events [6][7], or between normal and shear forces [8]. These sensors are more compact and require less external hardware, but provide only general information and usually lack localization.

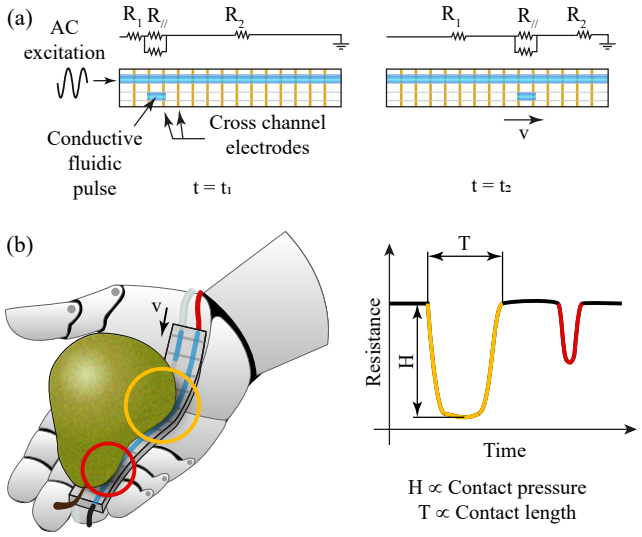

Fig. 1. Conceptual image of the pulsating fluidic sensor (PFS) and its sensing capabilities. (a) Schematic representation of the PFS and its electrical equivalent. (b) Demonstration of the PFS on a robotic hand to sense location, pressure and contact area of a gripped object and the resulting temporal change in resistance.

Traditionally object localization detection has been approached using sensor arrays to capture the spatial distribution of pressures, but these often require multiple active electrodes, fast processing speeds, and are not easily integrated into systems [9][10][11][12]. More recent approaches have relied on optimizing the placement of sensors and creating regions of targeted sensing, using a combination of software [13] and prior knowledge of the robot's application and potential movements [14][15][16]. These techniques have been implemented with the aim of limiting the number of sensors needed, and general bulkiness of the sensing setup. However, these strategies rely on knowing movements and behaviors beforehand, limiting their applicability across multiple users or for humans interacting with dynamic envi-

*This work was partially funded by The United Kingdom Engineering and Physical Sciences Research Council grant EP/S021035/1 and by a Department of Automatic Control and Systems Engineering, University of Sheffield, PhD scholarship

[1]Sheffield Biomedical Robotics Laboratory, Department of Automatic Control and Systems Engineering, University of Sheffield, S1 3JD, United Kingdom, e-mails: jjones8@sheffield.ac.uk, d.damian@sheffield.ac.uk

[2] Sheffield Robotics, University of Sheffield, UK

[3] Insigneo Institute for in silico Medicine, University of Sheffield, UK

ronments, where behaviors and reactions are unpredictable. For soft robots, work has also been done towards combining sensing and actuation to further limit the size of sensing elements [17][18], but again, the localization requires bulky external setups using multiple electrodes [19].

More recent work focusing on achieving localization within a minimal footprint has been carried out, using a variety of different modalities. Acoustic waveguides and optical ultrasound have been studied to investigate the detection of a variety of different stimuli, including strain and deformation, and have shown potential in localizing contacts, but require fast processing speeds [20][21]. Similarly, research using two pressure sensors at the ends of a closed air medium to locate fault events from signal timing has been conducted, but both the high frequency of data sampling needed and the difficulty detecting small non-damaging press forces present limitations [22]. Distributed magnetic sensing has also been used to transduce continuous deformation produced by stimuli, with relevance to localisation and shape reconstruction, but requires rigid external circuitry to be placed in close proximity to ensure operation [23][24]. Using fluidic sensing, some work has been conducted towards localization, using two parallel conductive channels with opposing sensitivities, and differentiating the varying stimuli from a comparison across the channels, but it is neither capable of detecting multiple stimuli events, nor characterizing the size and force of the press events [25]. Work using a single channel, with additional band-pass filter components embedded in the soft sensors, has also been demonstrated to distinguish location of events, but its compliance and scalability is compromised with the necessary additional rigid electronics [26]. There is therefore room for a scalable fluidic sensor with minimal hardware for localization of single and multiple press events.

In this work, we present a pulsating fluidic sensor (PFS) capable of distinguishing and differentiating between multiple press events of various forces, sizes and locations. Made up of just two parallel fluid channels and one pair of sensing electrodes, the PFSs present a compact and versatile solution for information-rich soft fluidic sensors. The soft PFS is also demonstrated in two sensing applications with relevance to rehabilitation and assistive wearables. The contributions of this paper include: (1) the concept, design and fabrication of a soft PFS; (2) the characterization of the PFS and its ability to distinguish between a variety of press events, varying in number, size, force and location; (3) the demonstration of the PFS in two applications of foot placement and grip location detection.

II. MATERIALS AND METHODS

A. Design concept of the soft PFS

The working principle of the soft PFS, shown in Fig. 1a, relies on two fluidic channels electrically connected with equidistant wires. One channel is fully filled with a conductive ionic liquid and excited using a sinusoidal electrical signal, while the other enables the flow of a conductive fluidic pulse (segment of ionic solution trapped between air gaps). During a press event, the cross-sectional area of both

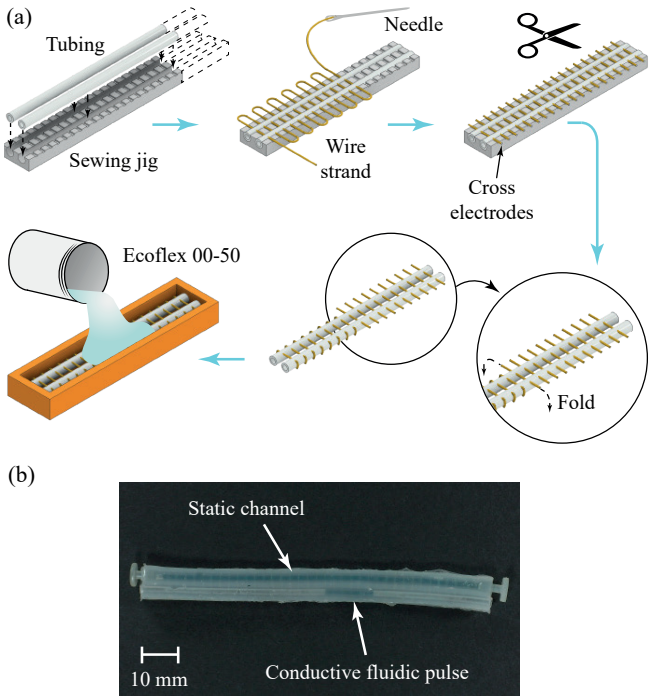

Fig. 2. Fabrication. (a) Schematic of the fabrication steps of the pulsating fluidic sensor (PFS) and (b) the final photo of the fabricated and filled PFS. The fabrication involves: fixing two lengths of silicone tubing into a custom sewing jig; evenly sewing wire across both tubings; trimming the edges of the wires to separate into individual electrodes; folding the electrodes over the tubings; and sealing and fixing the tubings with Ecoflex 00-50.

channels is reduced and when the pulse passes through this area, the difference in resistance is amplified. The location and size the press events cause direct changes in the timing, and duration of resistance spikes respectively. In addition, the larger the force being applied on the sensor, the greater the amplitude of the spikes. Furthermore, for multiple pressure points, the number of resistance spikes increases, and the location of these spikes is reflected in their timing.

The sensor can be modeled as a simple resistive network as shown in Fig. 1a. Thus, this pulsating fluidic conductive circuit allows the spatio-temporal identification of external stimuli deforming the sensor, by inducing resistance changes during its travel along the channel (Fig. 1b).

B. Fabrication of PFS

The fabrication begins by fixing two lengths of silicone tubing (ID:1.5 mm and OD:2.5 mm) into a sewing jig, designed to aid with aligning the elements of the sensor. A length of thin copper wire is then sewn across both silicone tubes in a zig-zag pattern spaced 2.5 mm apart. After the excess loops of wire are cut to separate the electrodes, the connected tubes are carefully removed from the jig and the ends of each electrode are folded over the tubing. Both tubes with the connecting electrodes are subsequently fixed in a resin 3D-printed mold (Form 3, Formlabs) and Ecoflex 00-50 silicone is poured over the top for final sealing and fixing. Before being poured, the Ecoflex 00-50 is first mixed in a mechanical mixer (ARE-249 Mixer, Thinky), and then

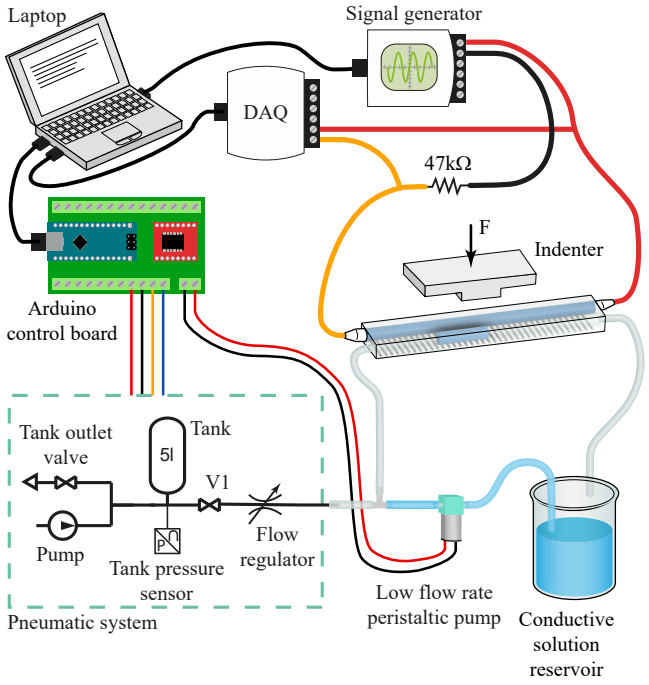

Fig. 3. Experimental setup. The experimental setup consists of the sensor connected fluidically to a peristaltic pump generating the fluidic pulses along with a pneumatic system driving the flow of the pulse, and electrically connected to a voltage divider circuit supplied by a signal generator and monitored with a DAQ. Throughout the experiments the sensor is pressed with a rectangular indenter, with varying forces, indent sizes and across multiple locations.

degassed for three minutes. Once poured, the Ecoflex 00-50 is left to cure at room temperature (approx. 20 °C) for at least three hours. Finally, the sensor is removed from the mold, the tubing ends are trimmed, and the sensor is filled with an ionic solution (9 g salt for 1 L distilled water). The first channel is completely filled with the ionic solution and plugged with electrodes on both ends. The second channel is left empty and is connected to a fluidic setup and two timing electrodes that enable the tracking of the fluidic pulse throughout the experiments. The fabrication steps are shown in Fig. 2.

C. Characterization Setup and Experimental Protocols

The full experimental setup used is shown in Fig. 3. The experimental setup consists of the PFS under testing, a signal generator and a data acquisition board (DAQ) connected to sensing and timing electrodes, as well as a custom-built pressure-driven flow control system for the fluidic pulse. A 5 N tensile test machine (Imada) or calibrated weights were used to carry out the press events and monitor the force amplitude of the press, as well as carry out different lengths and numbers of presses using a variety of custom attachments. During the press events the sensor itself was connected to multiple electrodes, to monitor changes in resistance and to track the fluidic pulse. The fully filled channel was plugged by two electrodes, supplied with a 1 V, 1 kHz sine wave and monitored using a custom-built DAQ acquiring the signal at 20 kHz. The fluidic pulse was also tracked by two extra pairs of electrodes at both the

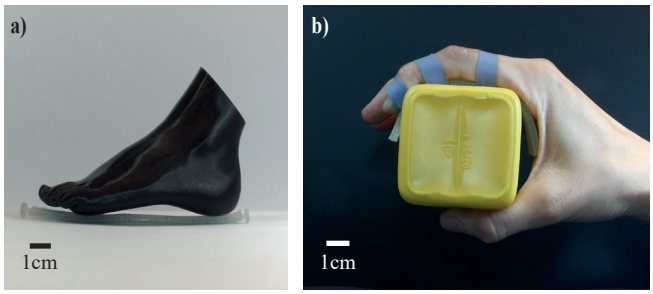

Fig. 4. Photos of application setups (a) Probing foot stance abnormalities, where A 3D printed foot is placed on the PFS. (b) Probing gripping with a PFS-embedded finger wearable. For the foot placement detection application, the foot was weighted evenly, on the toe and the heel and the location of the pressure was determined. For the grip location detection application, a cuboid object was gripped at varying angles and the location of the interaction of the finger with the object was determined.

inlet and outlet, connected to the same signal generator and DAQ. The purpose of these was to calibrate the timing of the saline solution segment, but are surplus to requirements. Finally throughout the experiments, a pneumatic setup was used to push the fluid segment generated by a peristaltic pump (Dolomite) at an average speed of 2.3 cm/s. This was achieved by pressurizing a 5 L reservoir tank to 60 kPa and reducing the pressure with a flow regulator as shown in Fig. 3.

The PFSs were tested under multiple press conditions, using a rectangular indenter, including different locations, sizes and force amplitudes of press. Five different press forces of 1 N to 5 N in 1 N increments were examined (same press size), as well as four different press sizes of 0.5, 1, 2 and 3 cm wide, each pressed down with 50 kPa. Five different press locations, from 1 cm to 9 cm evenly spaced by 2 cm, across the sensor (press force of 5 N) and multiple simultaneous press events were also tested on the PFS. These different conditions were chosen to show off the sensing and location capabilities of the PFSs.

D. Applications

After its characterization, the sensor was tested in two applications: a foot placement detection and a grip location detection, with potential to determine stance and grip abnormalities respectively, applicable in rehabilitation scenarios. For the foot placement detection, a single sensor was tested underneath a 3D printed foot model and manually weighted. An even foot weighting, a toe and a heel foot weighting were tested and compared with an unloaded sensor. For the grip location detection, a single sensor was fixed to the underside of a human index finger, and the sensor was tested on both a straight and curved finger, as well as when gripping a cuboid object between the fingertip and the thumb, the proximal phalanx and the thumb and finally between the distal and proximal phalanges and the thumb.

III. MODELING

The sensor can be modeled with a simplified electrical equivalent consisting of a series of resistors with one resistor in parallel, with each resistor governed by Pouillet's law.

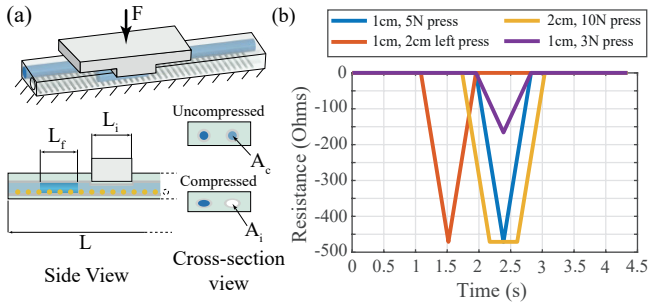

Fig. 5. Model. (a) Schematic of the sensor undergoing indent and key parameters. (b) Modeling results for different locations, sizes and forces of indents. Applying forces 2 cm further left results in a shifting of the time signal, applying wider indents results in a resistance spike longer in duration and applying smaller forces reduces the amplitude of the spike.

The following assumptions for the model were made the length of the sensor is fixed; the liquid displaced by the press events is evenly distributed across the rest of the channel and assumed to be negligible; change in cross-sectional area of the channel from a press event is uniform across the width of the press. Throughout the travel of the pulse, when the fluidic pulse is not under the indent, the total resistance can be described by:

$$R_{tot} = (L_s - L_i - \alpha_f L_f)\frac{\rho_s}{A_c} + L_i\frac{\rho_s}{A_i} + \alpha_f L_f \frac{\rho_s}{2A_c} \quad (1)$$

where L_s is the length of the full sensor, L_i the length of the fluidic indent, L_f the length of the pulsating fluidic segment, α_f the proportional amount of the pulsating fluid in the system (varying from 0 to 1 as the pulse enters and reversely as it exits the system), ρ_s the conductivity of the saline solution, A_c the normal cross-sectional area of a single channel and A_i the cross-sectional area of a pressed channel.

When the pulse is under the indent, the total resistance can be summarised as:

$$R_{tot} = (L_s - L_i - (1-\alpha_{fi})L_f)\frac{\rho_s}{A_c} + (1-\alpha_{fi})L_f\frac{\rho_s}{2A_c} + \alpha_i L_i\frac{\rho_s}{A_i} + \alpha_{fi}L_f\frac{\rho_s}{2A_i} \quad (2)$$

where α_{fi} is the proportion of the pulsating fluid under the indent and α_i is the proportion of the indent without the pulsating fluid.

Using the empirically-derived values of conductivity and the change in cross-sectional area, a simulation of a few examples of the PFS behavior is shown in Fig. 5(b).

IV. RESULTS AND DISCUSSION

A. Detection of Press Sizes

A variety of different press sizes were tested and the results are shown in Fig. 6. Overall, for each size of press event there is a negative spike in resistance compared to the baseline with no press event. The duration of the spike increases as the press size increases, as the pulse experiences

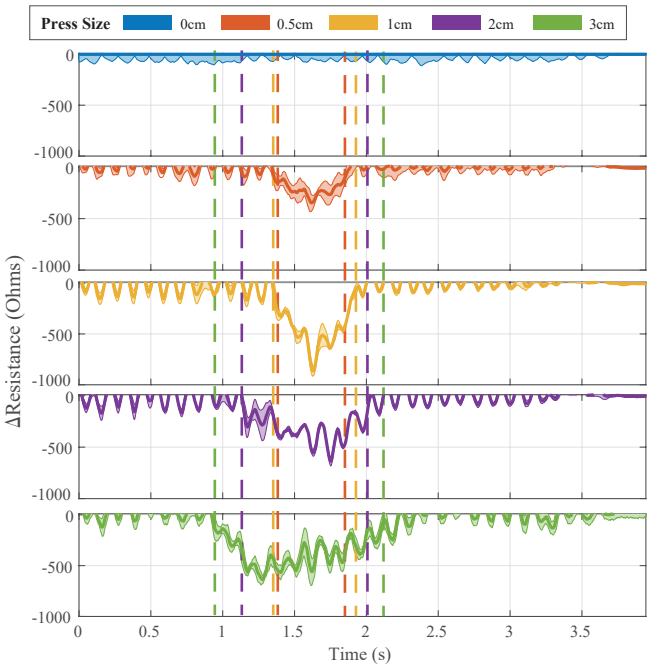

Fig. 6. Detection of press sizes. Various press sizes from 0 to 3 cm were tested. The average difference in resistance compared to the 0 cm press size and the standard deviation across five trials are shown.

a change in geometry for longer with the wider presses. Differences in press sizes of 1 cm or more can be differentiated, with clear distinctions between the 1, 2 and 3 cm press sizes. The variation in the amplitudes of the signals, despite the sensor bearing the same pressure, could be due to manufacturing errors or more uneven loading across the smaller surfaces. To conclude, the sensor shows a reasonable ability in distinguishing the size of press events.

B. Detection of Press Forces

The results from a variety of press force amplitudes from 0 to 5 N, on a 1 cm wide indent are shown in Fig. 7. The results show an increasing maximum drop in resistance as the force increases, visible across all press forces. An ANOVA test was carried out, which yielded that the minimum force that can be precisely identified among those tested is 2N, and similarly, the resolution of the PFS' force detection is 2N for forces under 3N, with the resolution increasing to 1N for forces higher than 3N. The resolution may prove larger if more granular force values were tested. The increased resolution for the larger forces could be explained by the tubing becoming more pronouncedly deformed beyond a threshold force. These large noise spikes result from the design with the cross-sectional electrodes being unevenly periodically connected as the pulse travels through the channel. Increasing the number of cross-electrodes would reduce these noise spikes and increase the distinction between the force amplitudes. Overall, the sensor demonstrates an ability to distinguish between different press forces.

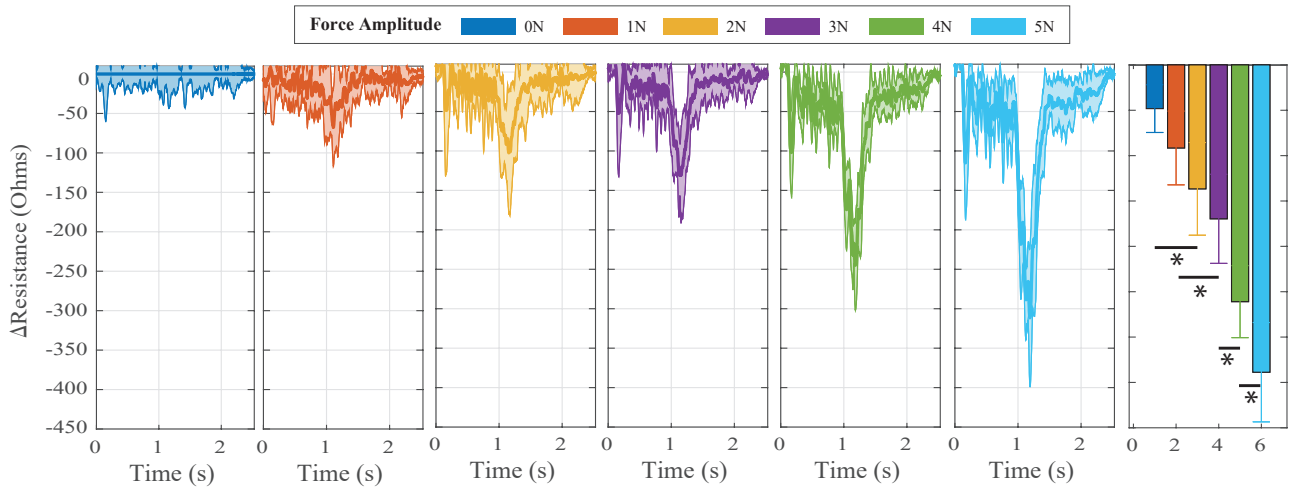

Fig. 7. Detection of press forces. Various press force amplitudes from 0 to 5 N were tested. The average difference in resistance compared to the 0 N press force and the standard deviation across five trials are shown. The asterisks in the bar chart highlight the closest neighboring conditions where the mean difference in resistance amplitude is statistically significant.

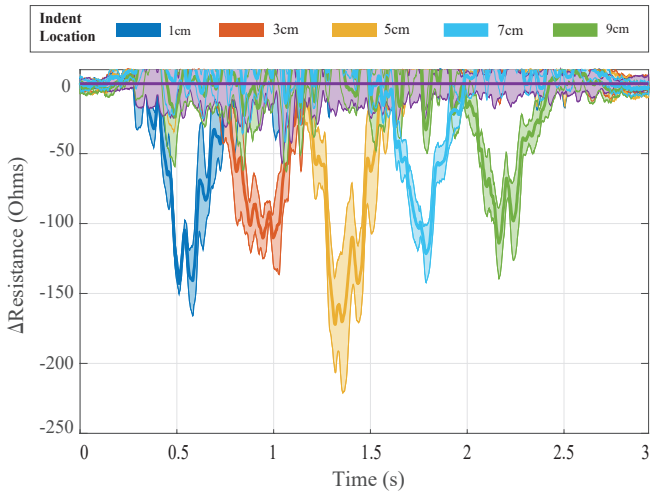

Fig. 8. Detection of press location. Various press press locations, from 1 cm to 9 cm evenly spaced by 2 cm across the PFS, were tested. The average difference in resistance compared to a no press average and the standard deviation across five trials are shown.

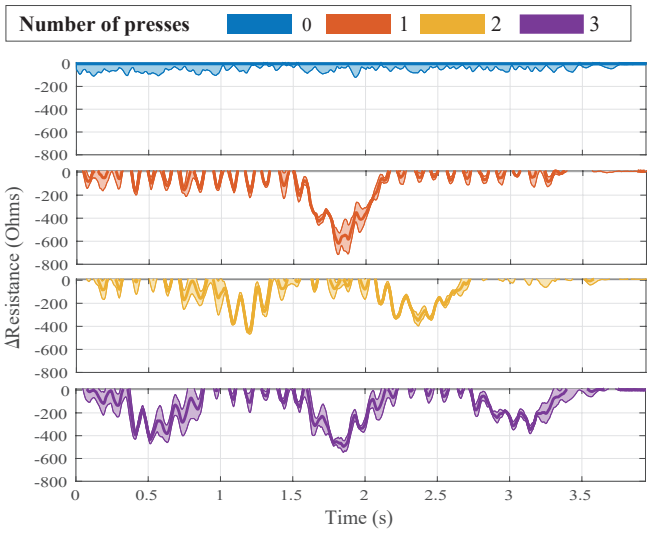

Fig. 9. Detection of multiple presses. One, two and three presses, each of 1 cm and spaced 2 cm apart, were tested. The average difference in resistance compared to a no press average and the standard deviation across five trials are shown.

C. Detection of Press Location

The location of a 5 N press with a 1 cm indent was tested across the length of the PFS and the results are shown in Fig. 8. The results show a good distinction between the different locations, with clear, and evenly spaced spikes across time, mirroring the evenly spaced indents tested. All of the spikes are similar in height, as would be expected, with the middle spike being the most pronounced at -250 Ω. The results demonstrate an ability to localize various press events from the timing of the spikes in resistance.

D. Detection of Multiple Presses

Building on the demonstration of using timing to identify location of indents, multiple indents were tested across the sensor and the results are shown in Fig. 9. An increasing number of press events from none to three were tested, each 1 cm in size, spaced evenly by 2 cm and loaded evenly with 50 kPa. From the results, subtracting the baseline change in resistance, the number of press events is clearly identifiable by the number of spikes in resistance. Additionally, the height of the spikes is similar across regardless of the number and similar for each of the conditions, with slight variations in peak resistance height from the experiments with two and three presses, likely due to uneven loading and distribution of the force across the indents. In general, the PFS demonstrated an ability to distinguish and locate multiple press events, exploiting the temporal changes experienced by the sensor as the fluid pulse travels along the sensor and amplifies notable changes in the geometry of the sensor.

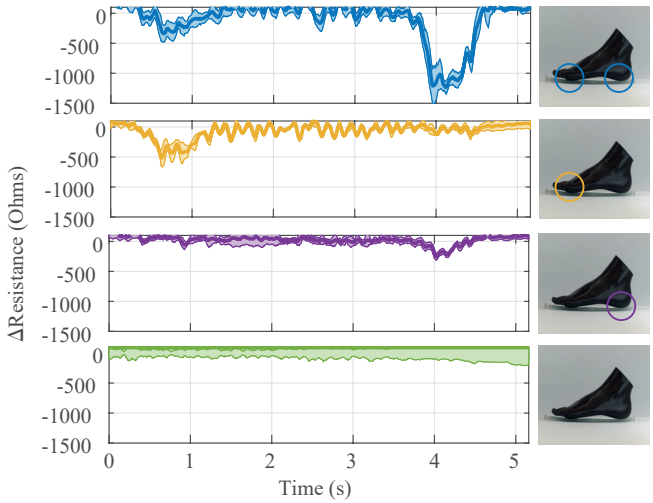

Fig. 10. Foot placement detection application. A 3D foot was weighted evenly, on the toe and on the heel. The average and standard deviation across three trials, relative to the baseline of an unloaded sensor, are shown.

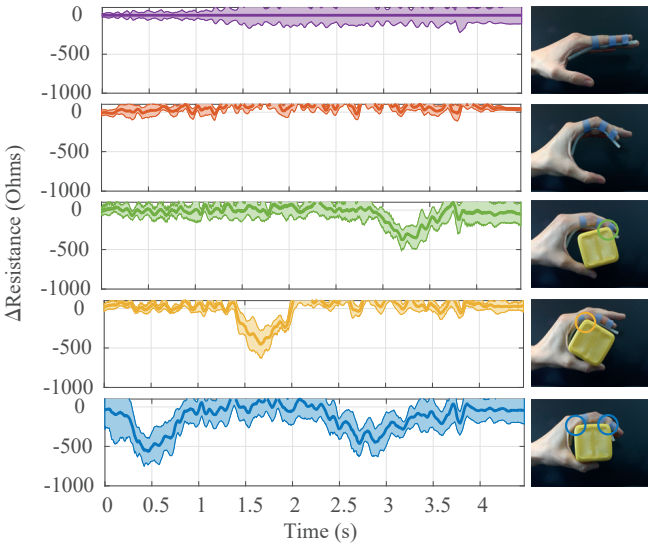

Fig. 11. Grip location detection application. A cuboid object was gripped at varying angles. The average and standard deviation across three trials, relative to the baseline of a straight finger, are shown.

V. Applications

Finally, the results from the two applications are shown in Fig. 10 and Fig. 11. For the foot placement detection, the results show peaks at the different foot locations that were weighted. For the evenly weighted foot, the results show two resistance spikes, with a larger spike of $-1500\,\Omega$ at the heel and a spike of $-500\,\Omega$ at the toe. For the toe weighted foot, the spike occurs at the earlier location, with a similar amplitude of around $-500\,\Omega$. For the heel weighted foot, the spikes occurs at the later location, but with a much decreased amplitude of around $-300\,\Omega$. The smaller spikes for the uneven weighted feet could be explained from the difficulty of manually weighting at an angle, as larger spikes compared to the even weighted foot would have been expected.

For the grip location detection, the results show varying numbers of peaks and locations of peaks, matching the number and different locations where the finger and the object touch. In the application, the conductive fluid pulse travels from the palm of the hand to the finger tip. The spikes in resistance across the different grips are around $-500\,\Omega$ and are sufficiently distinctive. Furthermore, curving the finger seemed to have little effect on the resistance, although stronger grips and curves might have a larger effect, with the more acute angles risking kinking and generally affecting the geometry of the channels.

VI. Conclusion and Future Work

To conclude, this work presents a compact yet information-rich soft sensor, which can be used to detect the number, the size, the force and the location of press events. The characterization highlighted the ability to localize single and multiple press events, by exploiting the spatio-temporal excitation of the system, as well as the potential to differentiate various sizes and force amplitudes of the press events. These characteristics were fully exploited and explored in the two applications presented, where the sensor was shown to be able to localize the weighting of a 3D printed foot, and distinguish between different grips, from the location of press event detection.

The overall sensor and setup does present some limitations. Notably the speed of the sensing, requiring on average 3 s to monitor the full 10 cm length of the sensor. Future work could include miniaturizing the channels further to achieve higher flow rates while maintaining laminar flow, therefore preserving the integrity of the conductive pulse. The use of extra conductive segments, with multiple running through the sensor, could also be explored to help increase the detection speed. Careful consideration of the size, distance and conductivity of the pulses would need to be taken though, to not lose localization information. The precision and accuracy of the system overall could be improved by using a laminated approach and disregarding the heavily manual steps. The increased control of the size and material of the channels would also enable tuning the sensor, with larger and/or more flexible channels more sensitive to lighter forces and vice versa for larger forces. Increasing the number of cross-electrodes or ultimately replacing the fully filled channel with a conductive elastic material, would improve both the signal-to-noise ratio and further minimize the overall size of the sensor. In addition to the sensor being miniaturized, the overall experimental setup also needs to be miniaturized further, using off-the-shelf fluidic pulse generators, to expand the potential applications to a greater number of robots. Finally, a next major step is the development of a reversible model to enable the prediction of the nature of the indentation from resistance changes, as well as its extension to more complex cases, such as overlapping events.

Acknowledgments

The authors would like to thank Kaan Esendağ for his help with photos.

REFERENCES

[1] M. Cianchetti, C. Laschi, A. Menciassi, and P. Dario, "Biomedical applications of soft robotics," *Nature Reviews Materials*, vol. 3, no. 6, pp. 143–153, 2018.

[2] H. Wang, M. Totaro, and L. Beccai, "Toward perceptive soft robots: Progress and challenges," *Advanced Science*, vol. 5, no. 9, p. 1800541, 2018.

[3] P. Polygerinos, N. Correll, S. A. Morin, B. Mosadegh, C. D. Onal, K. Petersen, M. Cianchetti, M. T. Tolley, and R. F. Shepherd, "Soft robotics: Review of fluid-driven intrinsically soft devices; manufacturing, sensing, control, and applications in human-robot interaction," *Advanced Engineering Materials*, vol. 19, no. 12, p. 1700016, 2017.

[4] B. Ward-Cherrier, N. Pestell, L. Cramphorn, B. Winstone, M. E. Giannaccini, J. Rossiter, and N. F. Lepora, "The tactip family: Soft optical tactile sensors with 3d-printed biomimetic morphologies," *Soft robotics*, vol. 5, no. 2, pp. 216–227, 2018.

[5] P. Roberts, M. Zadan, and C. Majidi, "Soft tactile sensing skins for robotics," *Current Robotics Reports*, vol. 2, pp. 343–354, 2021.

[6] T. Kim, S. Lee, T. Hong, G. Shin, T. Kim, and Y.-L. Park, "Heterogeneous sensing in a multifunctional soft sensor for human-robot interfaces," *Science robotics*, vol. 5, no. 49, p. eabc6878, 2020.

[7] A. Gupte, L. Kinnicutt, K. McDonald, and T. Ranzani, "A soft ionic sensor for simultaneous pressure and strain measurements," in *2020 3rd IEEE International Conference on Soft Robotics (RoboSoft)*, pp. 266–271, IEEE, 2020.

[8] D. M. Vogt, Y.-L. Park, and R. J. Wood, "Design and characterization of a soft multi-axis force sensor using embedded microfluidic channels," *IEEE sensors Journal*, vol. 13, no. 10, pp. 4056–4064, 2013.

[9] B. Shih, D. Shah, J. Li, T. G. Thuruthel, Y.-L. Park, F. Iida, Z. Bao, R. Kramer-Bottiglio, and M. T. Tolley, "Electronic skins and machine learning for intelligent soft robots," *Science Robotics*, vol. 5, no. 41, p. eaaz9239, 2020.

[10] B. Li, Y. Gao, A. Fontecchio, and Y. Visell, "Soft capacitive tactile sensing arrays fabricated via direct filament casting," *Smart Materials and Structures*, vol. 25, no. 7, p. 075009, 2016.

[11] A. Pagoli, F. Chapelle, J.-A. Corrales-Ramon, Y. Mezouar, and Y. Lapusta, "Large-area and low-cost force/tactile capacitive sensor for soft robotic applications," *Sensors*, vol. 22, no. 11, p. 4083, 2022.

[12] E. J. Markvicka, R. Tutika, M. D. Bartlett, and C. Majidi, "Soft electronic skin for multi-site damage detection and localization," *Advanced Functional Materials*, vol. 29, no. 29, p. 1900160, 2019.

[13] J. Tapia, E. Knoop, M. Mutnỳ, M. A. Otaduy, and M. Bächer, "Makesense: Automated sensor design for proprioceptive soft robots," *Soft robotics*, vol. 7, no. 3, pp. 332–345, 2020.

[14] U. Culha, U. Wani, S. G. Nurzaman, F. Clemens, and F. Iida, "Motion pattern discrimination for soft robots with morphologically flexible sensors," in *2014 IEEE/RSJ International Conference on Intelligent Robots and Systems*, pp. 567–572, IEEE, 2014.

[15] J.-B. Chossat, Y.-L. Park, R. J. Wood, and V. Duchaine, "A soft strain sensor based on ionic and metal liquids," *Ieee sensors journal*, vol. 13, no. 9, pp. 3405–3414, 2013.

[16] O. Shorthose, A. Albini, L. He, and P. Maiolino, "Design of a 3d-printed soft robotic hand with integrated distributed tactile sensing," *IEEE Robotics and Automation Letters*, vol. 7, no. 2, pp. 3945–3952, 2022.

[17] T. Helps and J. Rossiter, "Proprioceptive flexible fluidic actuators using conductive working fluids," *Soft Robotics*, vol. 5, no. 2, pp. 175–189, 2018.

[18] J. Jones and D. D. Damian, "A soft fluidic sensor-actuator for active sensing of force and displacement in biomedical applications," in *2022 IEEE/RSJ International Conference on Intelligent Robots and Systems (IROS)*, pp. 6913–6919, IEEE, 2022.

[19] P. Preechayasomboon and E. Rombokas, "Sensuator: A hybrid sensor–actuator approach to soft robotic proprioception using recurrent neural networks," in *Actuators*, vol. 10, p. 30, MDPI, 2021.

[20] W. Y. Choi, H. G. Jo, S. W. Kwon, Y. H. Kim, J. Y. Pyun, and K. K. Park, "Multipoint-detection strain sensor with a single electrode using optical ultrasound generated by carbon nanotubes," *Sensors*, vol. 19, no. 18, p. 3877, 2019.

[21] J.-B. Chossat and P. B. Shull, "Soft acoustic waveguides for strain, deformation, localization, and twist measurements," *IEEE Sensors Journal*, vol. 21, no. 1, pp. 222–230, 2020.

[22] T. George Thuruthel, A. W. Bosman, J. Hughes, and F. Iida, "Soft self-healing fluidic tactile sensors with damage detection and localization abilities," *Sensors*, vol. 21, no. 24, p. 8284, 2021.

[23] T. Hellebrekers, O. Kroemer, and C. Majidi, "Soft magnetic skin for continuous deformation sensing," *Advanced Intelligent Systems*, vol. 1, no. 4, p. 1900025, 2019.

[24] Y. Yan, Z. Hu, Z. Yang, W. Yuan, C. Song, J. Pan, and Y. Shen, "Soft magnetic skin for super-resolution tactile sensing with force self-decoupling," *Science Robotics*, vol. 6, no. 51, p. eabc8801, 2021.

[25] D. Kim and Y.-L. Park, "Contact localization and force estimation of soft tactile sensors using artificial intelligence," in *2018 IEEE/RSJ International Conference on Intelligent Robots and Systems (IROS)*, pp. 7480–7485, IEEE, 2018.

[26] J. Kim, S. Kim, and Y.-L. Park, "Single-input single-output multi-touch soft sensor systems using band-pass filters," *npj Flexible Electronics*, vol. 6, no. 1, p. 65, 2022.